Journal of Zhejiang University-SCIENCE A in press
www.jzus.zju.edu.cn; www.springer.com/journal/11582
E-mail: jzus_a@zju.edu.cn

Research Article
https://doi.org/10.1631/jzus.A2500365

Impact of UHI and global warming on multi-energy complementarity optimization of buildings: application to typical office buildings in Hangzhou, China

Qingqing MIAO[1,2,3], Xiaoyu LUO[1,2,3], Jiang LU[4], Weijun GAO[5], Yucong XUE[6], Yifan FAN[1,2,3], Jian GE[1,3]✉, Jiahong ZHAO[1,2,3]

[1]*College of Civil Engineering and Architecture, Zhejiang University, Hangzhou 310058, China*
[2]*Center of Balance Architecture, Zhejiang University, Hangzhou 310028, China*
[3]*Architectural Design and Research Institute Co. Ltd., Zhejiang University, Hangzhou 310028, China*
[4]*School of Civil Engineering and Architecture, Zhejiang University of Science and Technology, Hangzhou 310023, China*
[5]*Faculty of Environmental Engineering, The University of Kitakyushu, Kitakyushu 8080135, Japan*
[6]*China United Engineering Co. Ltd., Hangzhou 310056, China*

Abstract: Amid global warming and urbanization, building energy systems face the dual challenge of balancing growth in energy demand with environmental sustainability and resistance to future climate change. This study proposes a predictive framework that integrates the effects of future climate change and urban microclimate into energy consumption prediction and energy system optimization for typical office buildings in Hangzhou, China. First, optimal General Circulation Models (GCMs) from CMIP6 were selected through a performance evaluation, and statistical downscaling was employed to generate future typical meteorological year (TMY) data. Next, the Urban Weather Generator (UWG) was used to simulate urban heat island effects. Empirical formulas were applied to calculate urban wind speeds, while *DesignBuilder* was used to model solar radiation and hourly energy consumption. These data were then utilized to optimize the building energy system. The results reveal that future climate change significantly increases cooling demand (28.9%–103.0%) and reduces heating demand (19.7%–52.6%), with urban microclimates further amplifying these trends. The energy system optimization demonstrates that the net present value (NPV) of future climate and urban microclimate scenarios is 5.05%–16.65% higher than that of historical climate scenarios. Additionally, future climate scenarios result in higher peak energy demand, and thus necessitate larger system capacities to ensure reliability. While the initial required investment is higher, buildings optimized to account for global warming are more reliable and carry lower operational costs. We comprehensively quantify the effect of future urban microclimate on building energy systems, emphasizing its critical role in energy system planning, and providing insights for addressing the challenges of climate change and urbanization.

Key words: Future climate change; Urban microclimate; Building energy performance; Building energy system; Multi-objective optimization

1 Introduction

According to the Sixth Assessment Report of the Intergovernmental Panel on Climate Change (IPCC), under a high emissions scenario, the global average air temperature could increase by 3.3 °C to 5.7 °C by 2100, relative to the 1986–2005 period (IPCC, 2023). Such a rise would lead to a significant increase in the frequency of extreme weather events, resulting in severe climate and environmental impact (Li et al., 2024a). As a major carbon emitter globally, China bears significant responsibility for addressing climate change. At the 75th Session of the United Nations General Assembly, China pledged to achieve peak carbon emissions by 2030 and attain carbon neutrality by 2060 (Zhao et al., 2022). As one of the three major areas of energy consumption (industry, transportation, and buildings), the building sector accounts for a large portion of both direct and indirect carbon emissions

✉ Jian GE, gejian1@zju.edu.cn

Received July 31, 2025; Revision accepted Jan. 26, 2026;
Crosschecked

(Ashrafian, 2023; Chen et al., 2023). Therefore, enhancing energy efficiency and reducing emissions in the building sector is critical for addressing climate change and achieving sustainable development.

The configuration and operational optimization of building energy systems leveraging renewable energy is essential for enhancing building energy efficiency and reducing carbon emissions. However, optimization strategies for such energy systems are influenced by various factors. According to the International Energy Agency's Energy in Buildings and Communities Program (IEA-EBC) Annex 53, building energy use is determined by six parameters, including climate (Yoshino et al., 2017). Given that the typical lifespan of a building is between 50 and 70 years, its lifecycle will inevitably be affected by climate change (Guarino et al., 2022). These changes not only alter building energy demand but also impact the availability and reliability of renewable energy supplies. Specifically, future climate change driven by global warming will profoundly impact constructed environments. Meanwhile, with the acceleration of urbanization in China, human activities have altered meteorological conditions in urban areas (Yang et al., 2020), leading to a marked intensification of the urban heat island (UHI) effect. This has consequently elevated urban building energy demand and its fluctuations. Moreover, global warming and the UHI effect exhibit a mutually reinforcing relationship, which poses substantial challenges to sustainable energy transition efforts (Hosseini et al., 2022). A comprehensive understanding of variations in building energy consumption and renewable energy generation is essential for establishing lifecycle optimization strategies for building energy systems. Such strategies improve energy reliability for users while maximizing economic and environmental benefits.

Several studies have demonstrated that future climate change will lead to a significant increase in energy consumption across different climate zones and building types (Guan, 2009; Chan, 2011; Guan, 2012; Huang and Hwang, 2016). However, traditional energy system optimization models typically use existing meteorological or load data as inputs for design and optimization (Fathima and Palanisamy, 2015; Fazlollahi et al., 2015; Maroufmashat et al., 2015); this limits their ability to capture the potential impacts of future climate change on energy demand and supply. In recent years, researchers have increasingly recognized the importance of integrating climate change projections into energy system optimization, and have conducted studies on this topic. For instance, Zhang (2024) and Wang (2023) generated projected climate data using *Meteonorm* and *PRECIS*, respectively, then employed machine learning methods and *DeST* for load forecasting applied to integrated energy system optimization. Also, Ran et al. (2024a, 2024b) employed the morphing method to generate future climate data and used *EnergyPlus* to develop load forecasting models for typical days, which were then applied in a bi-level optimization of energy systems. Also, Perera et al. (2020, 2021, 2023) used *RCA4* (the 4th generation of the Rossby Centre Regional Climate Model) to obtain datasets for three future periods: a Typical Downscaled Year (TDY), an Extreme Cold Year (ECY), and an Extreme Warm Year (EWY). They then performed deterministic, robust, and stochastic optimization on energy systems.

However, due to mismatches in spatiotemporal resolution between climate and energy models, such approaches overlook the implications of future climate change on both the supply and demand sides of energy systems under the influence of urbanization. This study aims to comprehensively examine the combined effects of future climate change and urban climate, quantifying the impact of their uncertainties on energy system optimization strategies in order to enhance practicality and robustness.

The Coupled Model Intercomparison Project (CMIP) – initiated and organized by the Working Group on Coupled Modeling (WGCM) – plays a pivotal role in climate projection research. It is designed to assess the simulation capabilities of General Circulation Models (GCMs) and predict future climate change scenarios. This project has evolved into its sixth phase (CMIP6) (Jia et al., 2023), with four representative scenarios: SSP126, SSP245, SSP370, and SSP585. The project integrates numerous GCMs developed by multiple global institutions, and its results have been widely employed to assess the risks and impacts of future global and regional climate change. However, despite the excellent performance of GCMs at the global scale, uncertainties persist in their simulation results

due to differences in model initial conditions, spatial resolution, and in the ways different models account for local factors such as topography and vegetation. This leads to varying applicability of different GCMs across regions, thus necessitating evaluations of their applicability prior to use. Although there have been studies evaluating the applicability of GCMs from CMIP5 or CMIP6 across China (Xuan et al., 2017), there is still a lack of research on the applicability of GCMs from CMIP6 in the hot summer and cold winter zones of China. In addition, due to computational limitations, GCMs typically have a horizontal resolution ranging from 250 to 600 km; their simulation results have significant spatial resolution limitations at urban scales, making it difficult to effectively capture local climate characteristics (Hosseini et al., 2021). Therefore, further downscaling of GCMs is required to enhance both spatial and temporal resolution, in order to obtain hourly weather data for a specific region (Aliabadi and Mcleod, 2023). Current downscaling tools – such as *CCWorldWeatherGen* (Dias et al., 2020; Bell et al., 2022; Tamer et al., 2022), *WeatherShift* (Tootkaboni et al., 2021) and *Meteonorm* (Mauree et al., 2018; Ashrafian, 2023; Salvati and Kolokotroni, 2023) – use different climate data sources and downscaling methods to predict climate trends. However, these tools have not fully utilized the GCMs from CMIP6 and fail to evaluate the applicability of different GCMs across various regions (Rodrigues et al., 2023). To overcome the limitations of current tools, it is necessary to develop weather data prediction tools that can use the latest GCMs, and evaluate and flexibly select GCMs that meet the needs of building energy consumption simulations.

In urban microclimate research, scholars have increasingly recognized the scarcity of high-resolution climate data in the building sector. Thus, several studies have focused on simulating and analyzing urban microclimates to obtain more accurate weather data. Among these, Computational Fluid Dynamics (CFD)-based models have been widely applied to simulate urban climates (Zou et al., 2023). For example, Salvati et al. (2023) and Tsoka et al. (2021) used the *ENVI-met* model to generate future microclimate data. However, due to its high computational demands and long simulation times, *ENVI-met* is only suitable for small-scale simulations and has limitations when applied to larger spatial and temporal scales (Salvati et al., 2019). It is unable to provide the hourly weather data required for building energy performance simulations over an entire year. In addition to CFD models, the Urban Weather Generators (UWG) is also widely used to simulate urban climates (Litardo et al., 2020; Kamal et al., 2023). Although UWG can simulate the UHI effect, it only modifies air temperature and humidity data, without accounting for other key meteorological factors such as wind speed and solar radiation.

Overall, existing research lacks the integration of urban climate impacts into future climate change scenarios, in particular the effects of such climate change on the supply and demand sides of energy systems in the context of urbanization. Moreover, there is a lack of assessments of the applicability of the latest GCMs across different regions in climate research. Additionally, existing microclimate studies tend to focus on shorter time scales, which fail to meet the requirements for year-round energy consumption simulations. Therefore, in this study we aim to establish a future weather prediction framework in urban contexts and apply it to building energy system optimization. By focusing on the future climate change characteristics and urban microclimate features of a hot summer and cold winter zone in China – taking Hangzhou as a case study – we establish an accurate energy consumption prediction model. Based on this model, the impact of climate on renewable energy is considered, and an economic and environmentally friendly energy system lifecycle multi-objective optimization model is developed to ensure that the system adapts to future climate conditions.

This study is organized as follows. Section 2 presents the future climate, urban microclimate, and building energy system optimization models. Section 3 shows the results of the urban climate projections, and the impacts of climate change on building energy consumption and energy system life cycle optimization. Section 4 presents comparisons with other studies, and discusses the limitations and outlook for future work. Section 5 summarizes the findings and concludes the work.

2 Methodology

This section outlines the future climate prediction framework within an urban context, as well as the building energy system optimization strategy (Fig. 1). The framework begins by evaluating GCMs and selecting the best-performing model for downscaling in order to obtain regional-scale weather data, i.e., future TMY data. Next, UWG is used to generate air temperature and humidity data, considering the UHI effect. Then, urban wind speed is calculated to obtain urban microclimate data for the entire year. The generated weather data are integrated with a typical building model to produce annual energy consumption data, which are then used for lifecycle optimization of the building energy system.

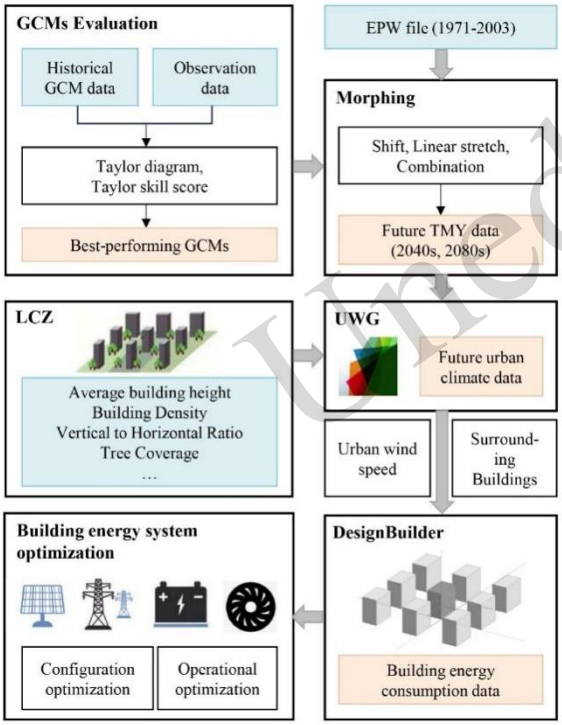

Fig. 1 Research framework

2.1 Future weather files

To overcome the spatial and temporal limitations of GCMs, we evaluate 12 GCMs using Taylor diagrams; the best-performing GCMs are statistically downscaled to obtain hourly weather data that accurately reflect local climate characteristics.

2.1.1 Climate zones

China is divided into seven climatic zones, with each zone characterized by similar climate conditions; this is essential for developing appropriate building design strategies (Ministry of Housing and Urban-Rural Development of the People's Republic of China, 1993). This study focuses on the climate change situation in the hot summer and cold winter zone of China. Since future climate research requires both typical meteorological year (TMY) files and historical measured monthly average air temperature data, five cities – Shanghai (121.45°E, 31.40°N), Changsha (112.92°, 26.33°N), Hangzhou (120.17°E, 30.23°N), Zhumadian (114.02°E, 33.00°N), and Chengdu (104.02°E, 30.67°N) – are selected as representatives of the hot summer and cold winter zone. These cities are used to evaluate the applicability of different GCMs in this climate zone.

2.1.2 GCM selection and evaluation

GCMs are complex model systems based on equations that predict climate change trends by simulating the interactions between the atmosphere, oceans, land surfaces, and ice sheets. As GCMs are used to predict both historical and future climate conditions, and studies have shown that air temperature has the greatest impact on building energy consumption among various meteorological parameters, we chose to quantitatively analyze historical monthly average air temperature data (1985–2014) obtained from *https://data.cma.cn/* and compare it with the simulated historical data from GCMs. The evaluation metrics we will use include the standard deviation (σ), root mean squared difference (RMSD), and correlation coefficient (R). The specific formulas are (Taylor, 2001):

$$\sigma_{\mathrm{o}} = \sqrt{\frac{\sum_{n=1}^{N}(O_n - \overline{O})^2}{\mathrm{N}}} \tag{1}$$

$$\sigma_{\mathrm{P}} = \sqrt{\frac{\sum_{n=1}^{\mathrm{N}}(P_n - \overline{P})^2}{\mathrm{N}}} \tag{2}$$

$$RMSD = \sqrt{\frac{\sum_{n=1}^{\mathrm{N}}\left((P_n - \overline{P}) - (O_n - \overline{O})\right)^2}{\mathrm{N}}} \tag{3}$$

$$R = \frac{\sum_{n=1}^{\mathrm{N}}(P_n - \overline{P})(O_n - \overline{O})}{\mathrm{N}\sigma_{\mathrm{o}}\sigma_{\mathrm{P}}} \tag{4}$$

where σ_{o} is the standard deviation at the observation site; σ_{P} is the standard deviation simulated by the GCM; O_n is the mean monthly air temperature measured at the observation site; P_n is the mean

monthly temperature simulated by the GCM; $\overline{O}$ is the mean air temperature measured at the observation site; and $\overline{P}$ is the mean air temperature simulated by the GCM.

Since the above statistical indicators conform to Eq. (5), a Taylor diagram (Taylor, 2001) can be used to simultaneously display the degree of similarity between the predicted values of different GCMs and the observed data for these indicators. In a Taylor diagram, if the simulated data are closer to the observed data, this indicates that the model performance is better. Therefore, the Taylor diagram provides a comprehensive view of the simulation results for the *CMIP6* models.

$$RMSD = \sigma_{\mathrm{o}}^2 + \sigma_{\mathrm{P}}^2 - 2\sigma_{\mathrm{o}}\sigma_{\mathrm{P}}R \tag{5}$$

In addition, the Taylor skill score (TSS) is introduced, as shown in Eq. (6) (Jia, et al., 2023), to quantify the correlation coefficient and standard deviation between the simulated and observed data; as such, it provides a quantitative assessment of the GCMs' simulation accuracy:

$$TSS = \frac{4(1+R)^4}{\left(\frac{\sigma_{\mathrm{P}}}{\sigma_{\mathrm{o}}}+\frac{\sigma_{\mathrm{o}}}{\sigma_{\mathrm{P}}}\right)^2(1+\mathrm{R_0})^4} \tag{6}$$

where R_0 is the maximum correlation coefficient that can be achieved between all the simulated and observed data. If the TSS is close to 1, this indicates that the GCM is better able to simulate the air temperature.

In this study, a total of 12 GCMs were selected with reference to existing studies (Xuan, et al., 2017; Jia, et al., 2023). The name, research organization, country, and resolution of each model are shown in Table S1.

2.1.3 Downscaling GCMs

Due to the spatial and temporal resolution limitations of GCMs, downscaling methods are needed to obtain future meteorological parameters that are representative of the regional scale but still have hourly resolution. By holistically considering the advantages, disadvantages, and applicability of the downscaling methods, the "morphing" method is used in this study to process the GCMs.

In the "morphing" method, the "baseline climate" is a prerequisite, which is defined as the average of the weather data over several years. Since TMY data represents long-term average weather conditions, it is used as the baseline climate in the "morphing" process. The Chinese Standard Weather Data (CSWD) is the TMY dataset with the largest number of stations and the longest time span (1971-2003). Therefore, CSWD data is selected for further processing in this study. The "Morphing" method includes three common transformations: shifting, linear stretching, and a combination of shifting and stretching (Belcher et al., 2005). The specific formulas are provided in Section S1.

2.2 Future urban microclimate

Existing TMY data are typically based on decades of historical observations from meteorological stations, which are often located at open sites such as airports; as such, this approach may not reflect the unique climatic phenomena of urban areas (Salvati and Kolokotroni, 2023). While the downscaling method discussed above has been used to overlay future climate change onto TMY data, it still relies on historical climate data from suburban meteorological stations and does not account for the impact of urbanization. Therefore, this section will develop a future urban microclimate prediction process based on Local Climate Zones (LCZ) theory, aimed at generating future hourly weather data that meet the input requirements for building energy performance simulation software.

2.2.1 Local Climate Zone

Traditional UHI research often simplifies analysis by separating urban and rural areas, and overlooking the complexity of urban surface features, which limits the detailed study of UHI effects (Shi et al., 2019). To address this, Stewart and Oke (2012) introduced the concept of LCZ, providing a more detailed description of the UHI effect on local climate (Boccalatte et al., 2023). Each LCZ type has unique attributes in terms of structure, land cover, and anthropogenic heat sources, which cause them to exhibit distinct air temperature characteristics under similar atmospheric conditions. The strong correlation between UHI intensity and LCZ classification has been well established (Beck et al.,

2018; Yin et al., 2024).

Meanwhile, the range of the LCZ definition aligns with the UWG, and the parameters provided by the LCZ system can meet the demands of the UWG for urban surface characteristics (Boccalatte, et al., 2023), enabling simulations of urban thermal environments. Since Hangzhou has the largest proportion of "open high-rise" type buildings, we choose LCZ4 to further study the impact of UHI (Yin, et al., 2024).

2.2.2 UHI effect

To account for the UHI effect in building energy performance simulations, Bueno et al. (2013) developed a UWG which uses meteorological data from suburban, airport, or rural stations to calculate air temperature and relative humidity within the urban canopy (Salvati and Kolokotroni, 2023). This UWG also considers the interactions between buildings and the urban climate.

The UWG is based on the basic physical laws of energy balance and heat transfer, and consists of four core modules: the Rural Station Model (RSM), Vertical Diffusion Model (VDM), Urban Boundary Layer Model (UBL), and Urban Canopy and Building Energy Model (UC-BEM). These modules are coupled with one other to simulate the urban microclimate (Bueno et al., 2013). The input data of the UWG include suburban weather files in EPW format and urban parameter files in XML format (Kamal et al., 2023). In this study, the future climate data obtained through downscaling in Section 2.1.3 served as the EPW-formatted suburban meteorological input data for the UWG, generating future urban climate files. Based on the LCZ described in Section 2.2.1, relevant urban parameters of the Hangzhou area are obtained from The World Urban Database and Access Portal Tools (WUDAPT). Specific parameters of this setup are detailed in Table S2, and the building model is shown in Fig. S1.

2.2.3 Urban wind speed

Urban wind speed is typically influenced by the building density and surface roughness of the city as compared with the wind speed near suburban weather stations, resulting in a lower wind speed. Numerous studies have developed empirical models to estimate urban wind speed using data from suburban weather stations (Macdonald et al., 1998; Georgakis and Santamouris, 2008; Santamouris et al., 2008; Nikkho et al., 2017; Lv et al., 2022). Among these, the power law presents a simple mathematical expression that can be applied across various conditions (Li et al., 2024b). *EnergyPlus* provides an equation similar to the power law for developing wind speed profiles based on terrain types (U.S. Department of Energy, 2021). In the present study, this power law is utilized to calculate urban wind speed as follows:

$$V_z = V_{\mathrm{met}}\left(\frac{\delta_{\mathrm{met}}}{z_{\mathrm{met}}}\right)^{\alpha_{\mathrm{met}}}\left(\frac{z}{\delta}\right)^{\alpha} \tag{7}$$

where z is the height above the ground (m); V_z is the wind speed at altitude z (m/s); α is the wind speed profile exponent at the site; δ is the wind speed profile boundary layer thickness at the site (m); z_{met} is the height above ground of the wind speed sensor at the meteorological station (m); V_{met} is the wind speed measured at the meteorological station (m/s); α_{met} is the wind speed profile exponent at the meteorological station; and δ_{met} is the wind speed profile boundary layer thickness at the meteorological station. Typical values for α and δ are listed in Table 1.

Table 1 List of coefficients related to wind speed profile

Terrain Description	Exponent α	Boundary Layer Thickness δ (m)
Flat, open country	0.14	270
Rough, wooded country	0.22	370
Towns and cities	0.33	460
Ocean	0.10	210
Urban, industrial, forest	0.22	370

2.3 Building energy model

This section outlines the development of a prototype model for a typical office building, and the simulation method for building energy consumption. Based on previous studies, a representative large office building model is established. Furthermore, considering the complex geometric structure of urban areas and the corresponding impact on building energy consumption, we use *DesignBuilder* [v.7.0.2, DesignBuilder Software Ltd., UK] to create a building cluster model that can assess the influence of the urban environment on building energy consumption.

2.3.1 Building model prototypes

We explore prototype building models to represent the typical urban building characteristics for specific building types and construction years (An et al., 2023). Since office buildings have higher feasibility for the application of multi-energy complementary systems compared to residential buildings, we reference the geometric information of 20 prototype building models developed by Yang et al. (2024), using a large office building as an example for simulation. Thermal parameters are referenced from the Ministry of Housing and Urban-Rural Development of China (2017). The specific parameters are shown in Table S3. Parameters such as switching time and utilization rate of internal loads like lighting, air conditioning, and electrical equipment are also referenced from the Ministry of Housing and Urban-Rural Development of China (2015).

2.3.2 Building energy simulation

The complex geometry of urban areas reduces solar radiation through mutual shading and decreases the sky view factor, limiting radiative cooling. Additionally, solar and long-wave radiation reflect between adjacent building surfaces, intensifying heat and further affecting the thermal environment. Solar radiation consists of direct, diffuse, and mutual reflections. While most building energy simulation software accounts for shading effects, simulating reflection between building surfaces requires geometric simulations and surface albedo data. *DesignBuilder*, however, includes a "reflection option" for simulating mutual reflections between buildings (Lauzet et al., 2019). Therefore, it is chosen in this study to create the building cluster model.

2.4 Building energy system optimization

In the face of climate change and growing energy demands, optimizing building energy systems is crucial for achieving sustainable development. This section focuses on the economic and environmental aspects of building energy systems. Mathematical models are developed for components including photovoltaics (PV), energy storage, and micro gas turbines (MG). Then, a lifecycle optimization model for the building energy system is established considering power balance constraints and the outputs of each generation unit, so as to optimize both the design and operational strategies.

2.4.1 Configuration optimization

The *HOMER Pro* [v.3.14.2, HOMER Energy, USA] software developed by the National Renewable Energy Laboratory (NREL) is used to design and analyze the optimization of various configurations of renewable and non-renewable energy components in the energy system. *HOMER Pro* uses heuristic algorithms to solve optimization problems for hybrid energy systems. Specifically, it employs enumeration to test and evaluate all possible system configurations (Al-Sharafi et al., 2017), ranking them based on the lowest net present cost (NPC) (Abdin and Mérida, 2019). In this study, *HOMER Pro* is applied for system modeling and simulation.

The optimization of the configuration of the building energy system components needs to be based on the meteorological conditions and grid information of the location. The building energy system components in this study include PV, storage batteries, and MG, and are operated in a grid-connected mode. Details on the software input are given in Section S2.

2.4.2 Operational optimization

Most current energy system operation optimization studies focus primarily on economic objectives, often neglecting environmental pollution concerns (Luo et al., 2020; Mathiesen et al., 2021). This study integrates both operational costs and environmental treatment costs to develop an optimization model for a building energy system, with the objective of minimizing total costs. The optimization problem will be solved using mixed integer linear programming (MILP).

To calculate the optimization objective, the power generation capacity of the PV, the MG, and the energy interaction of the energy storage system must first be evaluated. Therefore, we begin by developing models for PV, energy storage, and MG. The specific model is described in Section S3.

The operation optimization model of the building energy system considers both economic and environmental benefits. Based on the predicted 24 h electrical load and photovoltaic output curves, the model aims to minimize the total daily operational

cost of the system by coordinating the output of controllable units within the constraints of the system components. The operating costs considered in this study primarily include fuel consumption costs, maintenance costs, and interaction costs with the public grid; the environmental objectives use the pollutant treatment costs. To balance these two objectives, the multi-objective optimization problem is transformed into a single-objective problem by constructing and minimizing a composite cost function that integrates both aspects (Li et al., 2021). The specific formulas are:

$$\min(Z) = f_1 + f_2 \tag{8}$$

$$f_1 = \sum_{t=1}^{\mathrm{T}} C_{\mathrm{grid}}(t) + C_{\mathrm{MT}}(t) + C_{\mathrm{bess}}(t) + C_{\mathrm{f}}(t) \tag{9}$$

$$f_2 = \sum_{t=1}^{\mathrm{T}} C_{\mathrm{grid.en}}(t) + C_{\mathrm{MT.en}}(t) \tag{10}$$

where Z is the total cost; T is the period of operation optimization, being 24 h; f_1 is the daily operating cost; $C_{\mathrm{grid}}(t)$, $C_{\mathrm{MT}}(t)$, and $C_{\mathrm{bess}}(t)$ are the total cost of interacting with the grid at moment t, the O&M cost of the MG, and the O&M cost of the energy storage, respectively; $C_{\mathrm{f}}(t)$ is the cost of fuel consumption converted to per kWh at moment t; f_2 is the daily pollutant treatment cost; and $C_{\mathrm{grid.en}}(t)$ and $C_{\mathrm{MT.en}}(t)$ are the pollutant treatment costs of the grid and the MG, respectively.

To ensure the stability of the operation of the building energy system and the reasonability of the optimization, beyond ensuring the power balance in the energy system, each output unit, energy storage device, linking-up road, among other components must also meet certain constraints given in Section S4 (Conti et al., 2012).

3 Results

3.1 Selection of the global climate model

In this study, the historical prediction data of GCMs in five typical cities in the hot summer and cold winter zone of China are evaluated, investigating the effectiveness of different models in predicting the air temperature. From the Taylor diagram (Fig. S2), it can be seen that the correlation coefficients of all models in different cities essentially exceed 0.95, which represents a strong correlation. However, the applicability of the same GCM in different cities is not the same, and the optimal models in varying cities are different. For instance, the optimal model for Shanghai is MRI-ESM2-ESM2-0, the optimal model for Changsha and Zhumadian is GFDL-ESM4, the optimal model for Hangzhou is INM-CM5-0, the optimal model for Chengdu is ACCESS-ESM1-5, and the model that has the best combined effect in the five regions is CESM2-WACCM.

The Taylor skill score (TSS) was calculated for each model and ranked for each city as shown in Table S4. The best models for the different cities also vary. In order to determine the model that makes satisfactory evaluations throughout the hot summer and cold winter zone, we select the top three models based on the ranking results of the combined effects, which are CESM2-WACCM, GFDL-ESM4, and CMCC-CM2-SR5.

In order to predict the air temperature in the hot summer and cold winter region more accurately, the three preferred GCMs screened by the evaluation and the twelve GCMs are taken as equally weighted ensembles and compared with the prediction results of individual GCMs; the results are presented in Fig. S3. The preferred GCM ensemble averages are closer to the observed values than other data, both in the typical city and in the whole hot summer and cold winter zone. Therefore, the ensemble average of the three preferred GCMs is used as the basis for subsequent statistical downscaling.

3.2 Future weather analysis

Next, the preferred GCM ensemble average and the statistical downscaling method in Section 2.1.3 are used to calculate the weather data for Hangzhou under different paths for the future TMY, in which the years 2021-2053 are represented by the 2040s, and the years 2061–2093 are represented by the 2080s. Fig. 2 shows the changes of the monthly mean air temperature of Hangzhou under the four future SSP paths, and it is clear that the air temperature is significantly affected by the change in CO_2 concentration. Across two future TMY periods, the monthly mean air temperature also shows an increasing trend as the paths shift from the low radiative forcing path (SSP126) to the high radiative

forcing fossil fuel-dominated path (SSP585), which is particularly significant in the 2080s. There is also a significant increase in air temperature with age compared to the historical data. In both the 2040s and 2080s, the highest monthly average air temperature occurs in August. Specifically, under SSP245, the August average air temperature in the 2040s is projected to reach 29.5 °C, while it increases to 29.8 °C under SSP585. In the 2080s, these values rise even higher to 30.8 °C and 32.3 °C, respectively, exceeding the historical average air temperature in August of 28.2 °C. Similar trends are observed in other months as well.

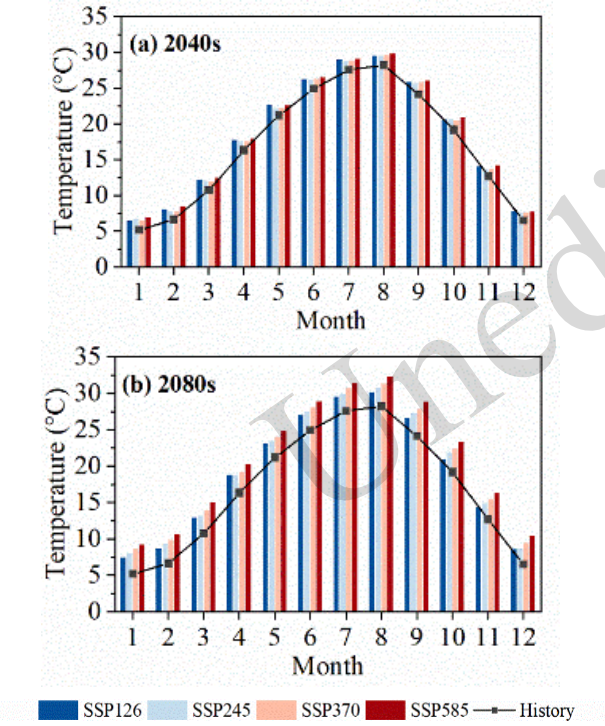

Fig. 2 Future monthly average air temperature change in Hangzhou under different paths in the (a) 2040s and (b) 2080s

The statistical downscaling method is based on historical TMY data, which is derived from suburban or rural weather stations and fails to reflect the impact of the urban environment on local climate. However, the UHI effect can have a significant impact on local climate and shows seasonal differences. Fig. S4 depicts the future UHI conditions in January and July at different ages under the SSP245 path. The air temperature in the city rises faster during the daytime due to dense urban buildings and subsurface factors; at night the air temperature in the city falls more slowly and is warmer due to the release of stored heat from urban buildings and surface materials. At midday, urban temperatures are slightly lower than rural temperatures. This is attributed to the high heat capacity of urban buildings and roads, which slows the temperature rise, as well as the shading effects of buildings. In the early morning, January urban temperatures are 1.9–2.9 °C higher than rural temperatures, while the July urban temperatures are 2.2–3.2 °C higher. At midday, January urban temperatures are approximately 0.2–0.6 °C lower than rural temperatures, and the July urban temperatures are about 0.1–0.2 °C lower. These findings are consistent with earlier studies (e.g. Akkose et al., 2021). From the 2040s to the 2080s, due to the increase in the rural temperature, the urban temperature increases accordingly; meanwhile, the UHI effect is slightly enhanced in the 2080s compared to the 2040s.

Fig. 3 shows the future climate (FC) and future urban microclimate (FUM) under different paths for the 2040s and 2080s. Compared with the FC, the FUM accounts for the role of urban morphological parameters (e.g., surface material and urban layout) on key meteorological parameters (e.g., air temperature and wind speed), presenting a more detailed characterization of urban climate change. Compared with the TMY and FC data, urban wind speeds are reduced by about 55% due to the combined effects of increased urban subsurface roughness, high building density, and building blockage.

Both future climate change and the UHI effect will lead to an increase in air temperature. Under the FC, the annual mean air temperatures of the different paths are significantly higher. Specifically, in the 2040s, the annual mean air temperature is projected to rise by 1.3–1.6 °C compared to historical levels, while in the 2080s, this increase ranges from 2–4 °C. Under the influence of the UHI effect, the annual mean air temperature in the 2040s will increase by an additional 1.4–1.5 °C compared to the FC, and in the 2080s, it will increase by 1.4–1.6 °C. The UHI effect further amplifies the impact of warming, with the maximum air temperature increasing by 1%–6% in the 2040s and 5%–11% in the 2080s under different pathways. The FUM reveals the critical role of urban forms in the future climate context, providing a

scientific basis for the development of targeted urban adaptation and mitigation strategies to meet the dual challenges of climate change and urbanization.

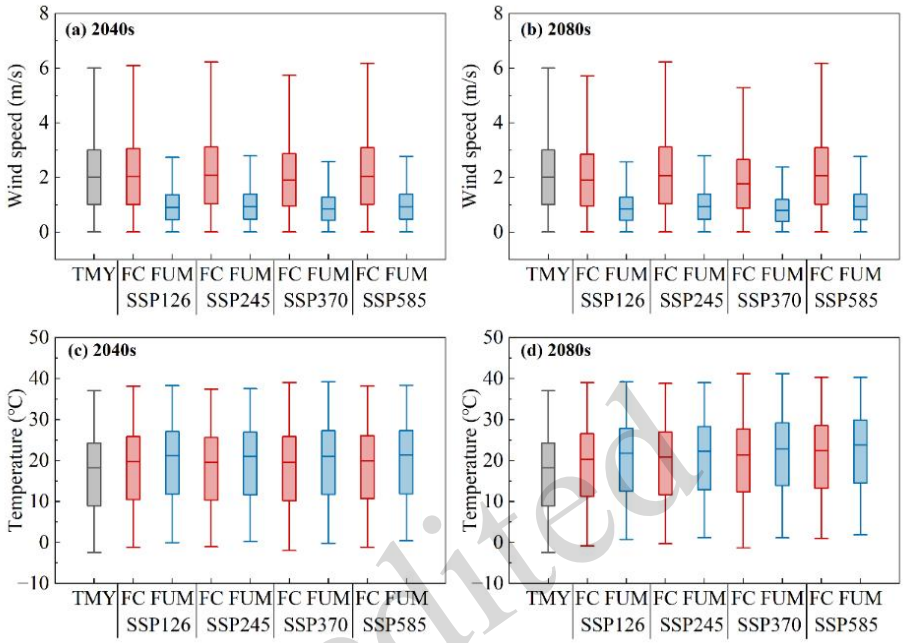

Fig. 3 The impacts of future climate change and future urban microclimate on temperature and wind speed under different paths: (a, b) wind speed in the 2040s and 2080s, (c, d) air temperature in the 2040s and 2080s. The upper and lower edges of the box plot represent the maximum and minimum values, respectively, and the line in the middle represents the median

3.3 Future climate impacts on energy demand

Fig. 4 illustrates the monthly variation of cooling and heating demand per unit area under historical TMY, FC, and FUM scenarios. The results show that the trends of cooling and heating demand for office buildings under FC and FUM are generally consistent with those under TMY, with the peak cooling demand occurring in June to September. Moreover, the ambient temperature increases year by year, leading to a corresponding rise in cooling demand for office buildings, while heating demand steadily declines.

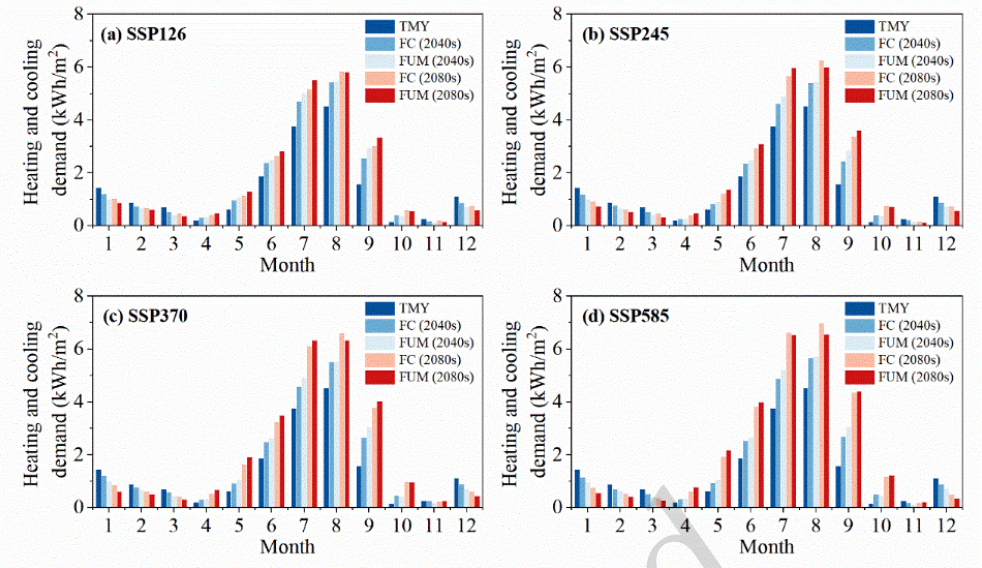

Fig. 4 Monthly changes in cooling and heating demand per unit area under different paths: (a) SSP126, (b) SSP245, (c) SSP370, (d) SSP585

Under the influence of the urban microclimate, the dense distribution of building clusters usually significantly reduces the amount of solar radiation reaching the building surfaces – especially during the summer months with high solar radiation. The shading effect not only reduces the amount of direct heat gain from facades and roofs, but also reduces the contribution of reflected radiation from the ground surface around the building, which in turn reduces the temperature increase at the building surface, leading to a reduction in cooling energy consumption. Additionally, the drop in wind speed decreases the heat removed by natural ventilation and also reduces convective heat transfer between the building exterior and the surrounding air, leading to an increase in cooling energy consumption. Although the UHI generally raises the urban temperature, its impact exhibits significant differences over time, with city temperatures being slightly lower than rural temperatures during the midday period. The factors above together result in lower cooling energy consumption in the FUM than in the FC in August in the 2080s. As the path increases, the difference between the cooling energy consumption in the FC and the cooling energy consumption in the FUM in August in the 2080s gradually increases to 0.03 kWh/m^2, 0.26 kWh/m^2, 0.28 kWh/m^2, and 0.42 kWh/m^2, respectively. Table 2 shows the impact of the shading effect of building clusters on building energy consumption for different paths in the 2080s. With the increase of the paths, the shading of building complexes can reduce the cooling energy consumption in August by 2.80%–4.48%. Meanwhile, the cooling energy consumption in FUM in August under different paths in the 2040s is higher than that in FC. This indicates that the contribution of the shading effect of the building complex to the reduction of cooling energy consumption gradually increases with higher temperatures.

Table 2 The impact of the shading of building complexes in the 2080s

Scenario	SSP 126	SSP 245	SSP 370	SSP 585
Energy consumption in August	-2.80%	-3.46%	-3.21%	-4.48%
Total energy consumption	-2.39%	-2.77%	-3.33%	-3.24%

Fig. 5 presents cooling and heating demand per unit area of a typical office building in Hangzhou under different paths of historical TMY, FC, and FUM. The further increases in temperature due to climate change and the UHI effect have a significant impact on building energy demand. Under the FC, cooling demand increases by 3.67–13.07 kWh/m^2, and heating demand decreases by 0.87–2.33 kWh/m^2

relative to TMY. Moreover, accounting for the urban effect will further increase cooling demand and decrease heating demand. The cooling energy consumption under the FUM increases by 4.55–13.29 kWh/m^2, and heating energy consumption decreases by 1.51–2.94 kWh/m^2 compared to the TMY.

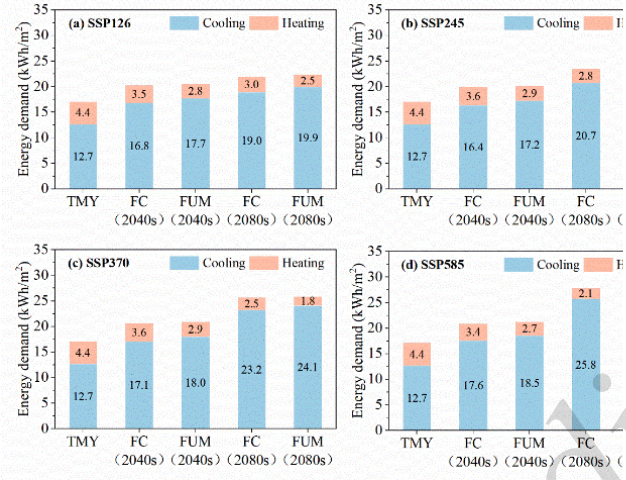

Fig. 5 Annual changes in cooling and heating demand per unit area under different paths: (a) SSP126, (b) SSP245, (c) SSP370, (d) SSP585

Section S5 presents the variations in cooling, heating, and overall energy demand. Comparing the energy consumption under the FC and FUM scenarios, the reduction in heating energy consumption outweighs the increase in cooling energy consumption due to the UHI effect, shading from buildings, and wind speed effects. Under the SSP585 scenario in the 2080s, the shading effect is more pronounced than in other paths, leading to a smaller increase in cooling energy consumption and a larger decrease in heating energy consumption. As a result, the total energy consumption in FUM is lower than in the FC scenario.

3.4 Energy system optimization results

3.4.1 The impact of climate on configuration

In this section we optimize the configuration of the energy system based on energy demand and energy supply under historical TMY, future climate, and future urban microclimate. Table S5 and Fig. 6 present the results of the configuration optimization under different climate scenarios. When considering FC and FUM, the NPV is 5.05%–16.65% higher than the optimal configuration results under the historical TMY. Meanwhile, the energy consumption under FC and FUM is 3.9%–14.96% higher than the historical TMY; this increase in demand is reflected in the energy system design and will be amplified, requiring higher capacity MG and battery energy storage to meet these needs. The use of historical configurations will not be able to meet energy demand in future climate scenarios. The results above therefore emphasize the importance of considering FC and FUM in energy system planning.

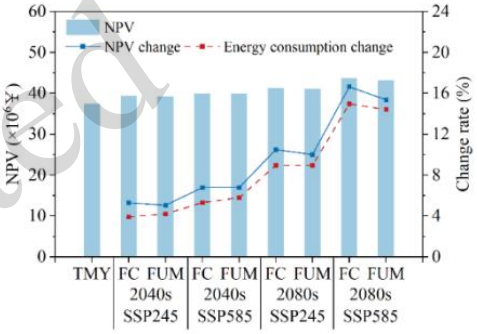

Fig. 6 Trends in NPV and energy consumption

3.4.2 The impact of climate on operations

The energy demand of office buildings is met by MG, PV, battery storage, and grid purchased power. Changes in energy demand in different scenarios, changes in electricity prices, and fluctuations in solar radiation all have an impact on the level of system output, which in turn affects operating costs. Fig. 7 depicts the system operating costs for typical days in each season for historical TMY, FC, and FUM for two paths. On a typical summer day, the energy consumption under both future climate scenarios is higher than under historical climate conditions, and this energy consumption gap increases over time. As a result, system operating costs also rise. Under SSP245, operating costs in the future scenarios are 4.7%–10.9% higher than those under historical TMY, while for SSP585, they are 5.9%–13.6% higher. The trend in operating costs on a typical winter day is the opposite of a typical summer day, as heating demand declines and system operating costs decrease over the years. Operating costs are 14.9%–26.3% lower in the

future scenarios than in the historical TMY for SSP245, and 16.6%–32.7% lower for SSP585. On a typical day in the transition season – which are times still dominated by cooling demand – operating costs follow the same trend as on typical summer day, being 40.1%–50.3% higher in SSP245 than in the historical TMY, and 42.4%–65.0% higher in SSP585. The complexities of the future climate and urban microclimate thus significantly affect the operating costs.

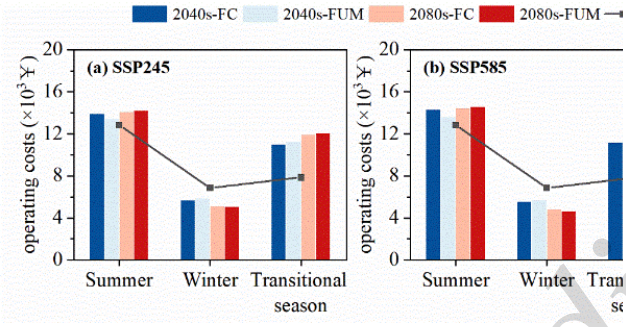

Fig. 7 A comparison of operating costs of building energy systems across seasons under (a) SSP245 and (b) SSP585

Table 3 lists the differences in energy consumption and operating costs for different scenarios in FC and FUM. In FC and FUM, the trend of operating cost changes in most scenarios is consistent with the change in energy consumption, i.e., when the energy consumption increases on a typical day, the operating cost also increases. However, it is worth noting that in specific scenarios – such as a typical summer day under the SSP245 pathway in the 2080s – the change in operating costs shows an opposite trend to the change in daily energy consumption. This is because under these scenarios, although daily energy consumption is higher in FUM than in FC, it only varies by 0.3% to 1.5% and the difference in energy consumption is relatively small. However, the increase in annual peak energy consumption in FC results in an increase in the capacity of the distributed energy system (see Section 3.4.1); this gives the system greater flexibility to respond more effectively to grid pricing strategies.

Table 3 Energy consumption and operating cost changes in future urban microclimates relative to the future climate

Scenario		Summer		Winter		Transitional season	
		Cost change (%)	Energy consumption change (%)	Cost change (%)	Energy consumption change (%)	Cost change (%)	Energy consumption change (%)
SSP245	2040s	-3.40	-3.97	3.06	-0.37	2.32	5.24
	2080s	1.09	-0.41	-2.04	-4.44	1.11	0.13
SSP585	2040s	-4.82	-4.95	2.78	-0.47	2.48	4.40
	2080s	1.08	-0.30	-4.28	-5.39	0.14	-1.44

In Fig. 8 we show the equipment operation on a typical winter day under SSP245 in the 2040s. With the increased capacity of the distributed energy system, the system's energy dispatch demonstrates more flexibility and efficiency during off-peak and peak electricity price periods. During off-peak periods (e.g., 6:00–8:00 and 12:00–13:00), the system purchases electricity from the grid to charge the battery, which not only provides a reserve for the load demand in the following hours, but also reduces the high cost of purchasing power during the peak price hours. During peak hours (e.g., 10:00–11:00 and 16:00–17:00), the energy storage system reduces the amount of power purchased from the grid by discharging the batteries, thereby reducing operating costs. In addition, excess electricity can be sold to the grid during peak hours, further optimizing the economics of the system. In future climate scenarios, changes in temperature and fluctuations in building loads may increase uncertainties in energy demand, but the larger energy storage capacity will enhance the system's ability to regulate this over time, further improving economic performance.

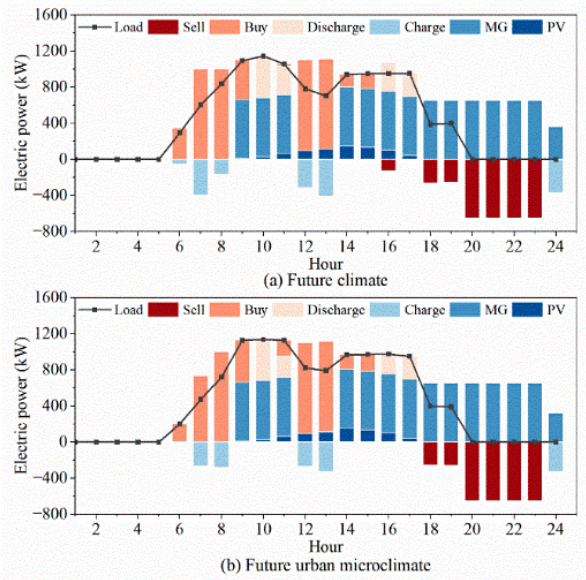

Fig. 8 Typical winter day operation for (a) future climate and (b) future urban microclimate under the SSP245 in the 2040s

4 Discussion

4.1 Comparison with existing studies

The downscaled climate results of this work align with those reported by Zou et al. (2021), who generated meteorological data for typical Chinese cities over 2020–2100 based on GCM data from CMIP5. The geographical proximity of Shanghai (their study) and Hangzhou (this study) provides a basis for comparison. Their findings indicate that the average temperature in Shanghai is projected to increase by 1.56–2.04 °C by the 2040s, and by 1.58–4.31 °C by the 2080s compared to TMY, which agrees with the results of this study.

For building energy consumption simulations, Chen et al. (2023) utilized the low-emission B1 scenario from the Fourth Assessment Report (AR4) of the IPCC to generate future climate data, which was applied to building energy consumption modeling in Changsha. As Changsha and Hangzhou are located within the same climate zone, their results offer an opportunity for comparison. Their findings revealed that, compared to the baseline year, energy consumption for typical large office buildings in Changsha increased by 1.93% in 2050 and 2.44% in 2080. However, their work relied on relatively outdated GCM data and considered only a single low-emission scenario, resulting in lower predicted energy consumption changes compared to our work. By incorporating the latest GCM data and accounting for multiple emission pathways, we provided more comprehensive and accurate energy consumption projections.

Regarding building energy system optimization, Perera et al. (2023) investigated the impact of high urban density and future climate change on energy system optimization. Due to differences in urban morphology parameters, their optimization results differ from those of this study. However, both investigations highlight that neglecting the effects of future climate change and urban climate in optimization processes can lead to energy shortages or wasted resources. Future climate change and urban climate are expected to significantly influence building heating, cooling, and overall energy consumption patterns. For Hangzhou, rising temperatures are projected to reduce winter heating demand but substantially increase summer cooling loads, thereby affecting the configuration and operations of energy systems. This study incorporated Hangzhou's specific climate conditions and future climate projections to analyze energy supply and demand variations under different scenarios. We proposed adaptive and robust energy system optimization strategies, providing a scientific basis for optimizing the energy systems of office buildings, in particular open high-rise buildings in the local climate zone of Hangzhou.

4.2 Mechanism analysis and mitigation strategies

By integrating GCM projections with urban microclimate modeling, we revealed that future typical office buildings in Hangzhou will likely exhibit surges in cooling demand, reductions in heating demand, and net increases in total energy consumption. These shifts are primarily driven by the superposition of rising background atmospheric temperatures and the urban thermal environment. On one hand, the temperature rise induced by global warming directly widens the indoor-outdoor thermal gradient, significantly exacerbating heat transfer through building envelopes. On the other hand, the UHI effect further amplifies this trend; high-thermal-capacity impervious surfaces within urban canyons and restricted Sky View Factors (SVF)

impede long-wave radiative cooling. This leads to persistent heat accumulation and necessitates prolonged high-load usage of air conditioning systems. Although the shading effect from building clusters mitigates solar heat gain to a certain extent, our simulation results indicate that the increased thermal load resulting from rising air temperatures outweighs the cooling load reduction provided by shading, ultimately resulting in a net increase in total energy consumption.

In terms of energy system optimization, load variations require adjustments in system configuration. The growth in energy demand and the elevation of peak loads compel the system to incorporate larger generation and energy storage capacities so as to satisfy reliability constraints, thereby increasing costs. Given that future technological advancements may reduce component costs and thus influence the optimization outcomes, we conducted a sensitivity analysis of this concept. While the cost of MG was assumed to be stable due to its technological maturity, investment costs for PV and energy storage were varied between -10% and -50%, based on NREL's Annual Technology Baseline (ATB) projections (National Renewable Energy Laboratory, 2024). The optimal capacity configuration of the system remained unchanged within this cost variation range. This indicates that climate-driven peak load and energy demand growth are the dominant determinants of system capacity. Meanwhile, as illustrated in Fig. 9, the NPV decreased with the reduction of investment costs, exhibiting higher sensitivity to PV cost variations. Consequently, the conclusion that future climate conditions require an expansion of system capacity is robust. Although capacity expansion is a necessary measure to cope with peak loads, future declines in equipment costs will further enhance the economic viability of such systems.

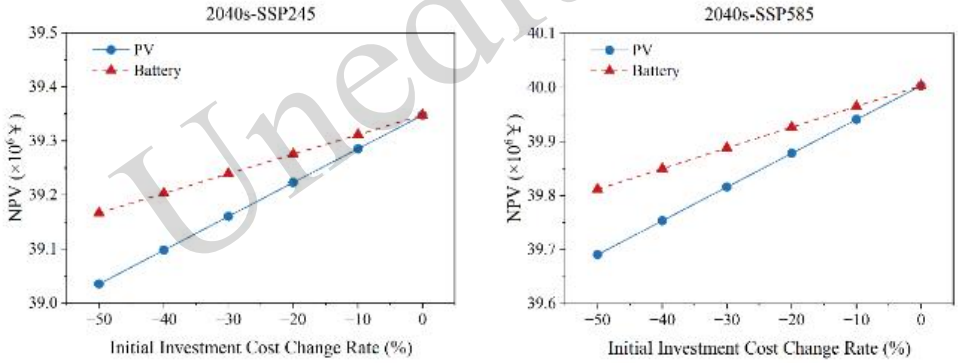

Fig. 9 The relationship curves between NPV and component cost change rate

Nevertheless, exclusive reliance on supply-side capacity expansion represents a passive adaptation approach. To fundamentally mitigate system stresses and ensure sustainability, a holistic framework encompassing source mitigation, environmental improvement, and peak shaving is imperative. First of all, the simulation results indicate that shifting towards higher-emission climate pathways leads to increased energy consumption, as well as higher NPV and operating costs for the energy system. Therefore, promoting a societal transition toward a sustainable pathway can curb background temperature increases at their source, and hold the increase in building energy consumption within manageable limits. Second, given that the UHI effect amplifies the impact of global warming, improving the urban microclimate is a critical strategy for energy conservation. We recommend extensively promoting vertical greenery, roof gardens, and high-albedo cool materials in future urban renewal projects. These measures would directly mitigate UHI intensity by enhancing evapotranspiration and reducing surface heat absorption, and also synergistically lower the cooling load of air conditioning systems through effective shading. Finally, since reducing peak energy consumption allows for lower energy system sizing, Demand Side Response (DSR) technologies should be integrated at the operational level. By leveraging the thermal inertia of office buildings and flexible load characteristics for peak shaving and valley filling,

the instantaneous peak loads triggered by extreme heat could be effectively smoothed.

4.3 Limitations and future work

A few limitations are present in this work. First, in terms of climate studies, the lack of long-term, high-quality historical solar radiation data for the study area necessitated the selection of GCMs based primarily on dry-bulb temperature. As solar radiation critically influences building energy demand and photovoltaic output, future work should incorporate comprehensive radiation datasets to enable a multivariate assessment of GCMs. Secondly, we utilized a statistical downscaling method to generate future TMY climate parameters. However, this did not account for the impact of extreme climate events. Such events could significantly increase heating and cooling demand in buildings and affect the power generation capacity of renewable energy systems (Bell et al., 2022). Future research should therefore incorporate simulations and analyses of extreme climate conditions to provide a more comprehensive assessment of energy system adaptability under diverse scenarios. Additionally, the impact of climate change on building energy performance will vary across different climate zones. Subsequent studies should thus investigate the adaptability of building energy systems to climate change across various regions.

Regarding energy system optimization, this study utilized *HOMER Pro* for configuration optimization, which involved certain assumptions about operational strategies. Different operational strategies could lead to varying configuration outcomes. Moreover, we made assumptions about grid electricity prices and equipment costs, without considering potential cost reductions driven by future technological advancements. Later research should consider the trend of technological advancement when analyzing the potential impacts of equipment cost reductions and changes in electricity prices on the optimization results; in this way, better guidance can be provided for practical applications.

5 Conclusions

In this study we established a framework for future climate prediction in urban contexts, and applied it towards building energy consumption forecasting and energy system optimization. The results showed that future climate change will lead to a 28.9%–103.0% increase in cooling demand, a 19.7%–52.6% decrease in heating demand, and a 3.9%–15.0% increase in total energy consumption for a typical office building in Hangzhou, China. Additionally, future urban microclimates are projected to further amplify these effects, increasing cooling demand while reducing heating demand. Climate change significantly impacts building energy demand, and its effects are reflected in the optimization of energy system configurations. Under future climate and urban microclimate conditions, the NPV of optimal system configurations is estimated to be 5.05%-16.65% higher than under historical climate conditions. Moreover, factors such as building shading, urban wind speeds, and the UHI effect contribute to peak energy consumption being higher under future climate conditions than under future urban microclimate conditions. This will result in the need for larger system capacities to ensure energy system reliability, which in turn further influences system operational costs. However, higher system capacities provide increased flexibility, enabling more effective cost reductions during operation.

Acknowledgments

This work is supported by the National Natural Science Foundation of China (52178093), “Pioneer” and “Leading Goose” R&D Program of Zhejiang (2023C03152) and “The Fundamental Research Funds for the Central Universities (226-2024-00212)”. The authors would also like to acknowledge the support provided by these projects, with the corresponding author recognized as a Qianjiang Distinguished Expert in Hangzhou.

Author contributions

Qingqing MIAO: Conceptualization, Data curation, Methodology, Writing - original draft, Writing - review and editing. Xiaoyu LUO: Supervision. Jiang LU: Supervision. Weijun GAO: Supervision. Yucong XUE: Writing – review and editing. Yifan FAN: Conceptualization, Methodology, Funding acquisition, Writing – review and editing. Jian GE: Project administration, Funding acquisition, Supervision. Jiahong ZHAO: Writing – review and editing.

Conflict of interest

Qingqing MIAO, Xiaoyu LUO, Jiang LU, Weijun GAO, Yucong XUE, Yifan FAN, Jian GE, and Jiahong ZHAO

declare that they have no conflict of interest.

References

Abdin Z, Mérida W, 2019. Hybrid energy systems for off-grid power supply and hydrogen production based on renewable energy: A techno-economic analysis. *Energy Conversion and Management*, 196:1068-1079. https://doi.org/10.1016/j.enconman.2019.06.068

Akkose G, Akgul CM, Dino IG, 2021. Educational building retrofit under climate change and urban heat island effect. *Journal of Building Engineering*, 40:18. https://doi.org/10.1016/j.jobe.2021.102294

Al-Sharafi A, Sahin AZ, Ayar T, et al., 2017. Techno-economic analysis and optimization of solar and wind energy systems for power generation and hydrogen production in saudi arabia. *Renewable & Sustainable Energy Reviews*, 69:33-49. https://doi.org/10.1016/j.rser.2016.11.157

Aliabadi AA, Mcleod RM, 2023. The vatic weather file generator (vwfg v1.0.0). *Journal of Building Engineering*, 67:18. https://doi.org/10.1016/j.jobe.2023.105966

An JJ, Wu Y, Gui CX, et al., 2023. Chinese prototype building models for simulating the energy performance of the nationwide building stock. *Building Simulation*, 16(8):1559-1582. https://doi.org/10.1007/s12273-023-1058-5

Ashrafian T, 2023. Enhancing school buildings energy efficiency under climate change: A comprehensive analysis of energy, cost, and comfort factors. *Journal of Building Engineering*, 80:27. https://doi.org/10.1016/j.jobe.2023.107969

Beck C, Straub A, Breitner S, et al., 2018. Air temperature characteristics of local climate zones in the augsburg urban area (bavaria, southern germany) under varying synoptic conditions. *Urban Climate*, 25:152-166. https://doi.org/10.1016/j.uclim.2018.04.007

Belcher SE, Hacker JN, Powell DS, 2005. Constructing design weather data for future climates. *Building Services Engineering Research & Technology*, 26(1):49–61. https://doi.org/10.1191/0143624405bt112oa

Bell NO, Bilbao JI, Kay M, et al., 2022. Future climate scenarios and their impact on heating, ventilation and air-conditioning system design and performance for commercial buildings for 2050. *Renewable & Sustainable Energy Reviews*, 162:16. https://doi.org/10.1016/j.rser.2022.112363

Boccalatte A, Fossa M, Thebault M, et al., 2023. Mapping the urban heat island at the territory scale: An unsupervised learning approach for urban planning applied to the canton of geneva. *Sustainable Cities and Society*, 96:17. https://doi.org/10.1016/j.scs.2023.104677

Bueno B, Norford L, Hidalgo J, et al., 2013. The urban weather generator. *Journal of Building Performance Simulation*, 6(4):269-281. https://doi.org/10.1080/19401493.2012.718797

Chan ALS, 2011. Developing future hourly weather files for studying the impact of climate change on building energy performance in hong kong. *Energy and Buildings*, 43(10):2860-2868. https://doi.org/10.1016/j.enbuild.2011.07.003

Chen YX, Ren ZY, Peng ZW, et al., 2023. Impacts of climate change and building energy efficiency improvement on city-scale building energy consumption. *Journal of Building Engineering*, 78:15. https://doi.org/10.1016/j.jobe.2023.107646

Conti S, Nicolosi R, Rizzo SA, et al., 2012. Optimal dispatching of distributed generators and storage systems for mv islanded microgrids. *IEEE Transactions on Power Delivery*, 27(3):1243-1251. https://doi.org/10.1109/TPWRD.2012.2194514

Dias JB, Da Graça GC, Soares PMM, 2020. Comparison of methodologies for generation of future weather data for building thermal energy simulation. *Energy and Buildings*, 206:16. https://doi.org/10.1016/j.enbuild.2019.109556

Fathima AH, Palanisamy K, 2015. Optimization in microgrids with hybrid energy systems - a review. *Renewable & Sustainable Energy Reviews*, 45:431-446. https://doi.org/10.1016/j.rser.2015.01.059

Fazlollahi S, Becker G, Ashouri A, et al., 2015. Multi-objective, multi-period optimization of district energy systems: Iv - a case study. *Energy*, 84:365-381. https://doi.org/10.1016/j.energy.2015.03.003

Georgakis C, Santamouris M, 2008. On the estimation of wind speed in urban canyons for ventilation purposes - part 1: Coupling between the undisturbed wind speed and the canyon wind. *Building and Environment*, 43(8):1404-1410. https://doi.org/10.1016/j.buildenv.2007.01.041

Guan L, 2009. Implication of global warming on air-conditioned office buildings in australia. *Building Research and Information*, 37(1):43-54. https://doi.org/10.1080/09613210802611025

Guan L, 2012. Energy use, indoor temperature and possible adaptation strategies for air-conditioned office buildings in face of global warming. *Building and Environment*, 55:8-19. https://doi.org/10.1016/j.buildenv.2011.11.013

Guarino F, Tumminia G, Longo S, et al., 2022. An integrated building energy simulation early-design tool for future heating and cooling demand assessment. *Energy Reports*, 8:10881-10894. https://doi.org/10.1016/j.egyr.2022.08.224

Hosseini M, Bigtashi A, Lee B, 2021. Generating future weather files under climate change scenarios to support building energy simulation - a machine learning approach. *Energy and Buildings*, 230:21. https://doi.org/10.1016/j.enbuild.2020.110543

Hosseini M, Javanroodi K, Nik VM, 2022. High-resolution impact assessment of climate change on building energy performance considering extreme weather events and microclimate - investigating variations in indoor thermal comfort and degree-days. *Sustainable Cities and Society*, 78:21. https://doi.org/10.1016/j.scs.2021.103634

Huang KT, Hwang RL, 2016. Future trends of residential building cooling energy and passive adaptation measures to counteract climate change: The case of taiwan. *Applied Energy*, 184:1230-1240. https://doi.org/10.1016/j.apenergy.2015.11.008

Ipcc, 2023. Climate change 2021 – the physical science basis: Working group i contribution to the sixth assessment report of the intergovernmental panel on climate change. Technical Report, Cambridge University Press,

Jia QM, Jia HF, Li YJ, et al., 2023. Applicability of cmip5 and cmip6 models in china: Reproducibility of historical simulation and uncertainty of future projection. *Journal of Climate*, 36(17):5809-5824. https://doi.org/10.1175/jcli-d-22-0375.1

Kamal A, Mahfouz A, Sezer N, et al., 2023. Investigation of urban heat island and climate change and their combined impact on building cooling demand in the hot and humid climate of qatar. *Urban Climate*, 52:18. https://doi.org/10.1016/j.uclim.2023.101704

Lauzet N, Rodler A, Musy M, et al., 2019. How building energy models take the local climate into account in an urban context - a review. *Renewable & Sustainable Energy Reviews*, 116:19. https://doi.org/10.1016/j.rser.2019.109390

Li JX, Zhang QQ, Etienne XL, 2024a. Optimal carbon emission reduction path of the building sector: Evidence from china. *Science of the Total Environment*, 919:17. https://doi.org/10.1016/j.scitotenv.2024.170553

Li Q, Chen JY, Luo XW, 2024b. Estimating omnidirectional urban vertical wind speed with direction-dependent building morphologies. *Energy and Buildings*, 303:15. https://doi.org/10.1016/j.enbuild.2023.113749

Li SY, 2020. Research on optimization operation of microgrid based on genetic simulated annealing particle swarm algorithm. Nanjing University of Posts and Telecommunications,

Li XS, Zhang J, He Y, et al., 2021. Multi-objective optimization dispatching of microgrid based on improved particle swarm algorithm. *Electric Power Science and Engineering*, 37(3):1-7. https://doi.org/10.3969/j.ISSN.1672-0792.2021.03.001

Litardo J, Palme M, Borbor-Cordova M, et al., 2020. Urban heat island intensity and buildings' energy needs in duran, ecuador: Simulation studies and proposal of mitigation strategies. *Sustainable Cities and Society*, 62:16. https://doi.org/10.1016/j.scs.2020.102387

Luo L, Abdulkareem SS, Rezvani A, et al., 2020. Optimal scheduling of a renewable based microgrid considering photovoltaic system and battery energy storage under uncertainty. *Journal of Energy Storage*, 28:12. https://doi.org/10.1016/j.est.2020.101306

Lv GQ, Zhao K, Qin YL, et al., 2022. An urban-scale method for building roofs available wind resource evaluation based on aerodynamic parameters of urban sublayer surfaces. *Sustainable Cities and Society*, 80:12. https://doi.org/10.1016/j.scs.2022.103790

Macdonald RW, Griffiths RF, Hall DJ, 1998. An improved method for the estimation of surface roughness of obstacle arrays. *Atmospheric Environment*, 32(11):1857-1864. https://doi.org/10.1016/s1352-2310(97)00403-2

Maroufmashat A, Elkamel A, Fowler M, et al., 2015. Modeling and optimization of a network of energy hubs to improve economic and emission considerations. *Energy*, 93:2546-2558. https://doi.org/10.1016/j.energy.2015.10.079

Mathiesen P, Stadler M, Kleissl J, et al., 2021. Techno-economic optimization of islanded microgrids considering intra-hour variability. *Applied Energy*, 304:11. https://doi.org/10.1016/j.apenergy.2021.117777

Mauree D, Coccolo S, Perera ATD, et al., 2018. A new framework to evaluate urban design using urban microclimatic modeling in future climatic conditions. *Sustainability*, 10(4):20. https://doi.org/10.3390/su10041134

Ministry of Housing and Urban-Rural Development of China, 2015. Design standard for energy efficiency of public buildings, GB 50189-2015.

Ministry of Housing and Urban-Rural Development of China, 2017. Development research on building energy efficiency standard and implementation roadmap of total energy consumption control in buildings. Technical Report,

Ministry of Housing and Urban-Rural Development of the People's Republic of China, 1993. Standard for climatic regionalization for architecture, GB 50178-93.

National Renewable Energy Laboratory. 2024. 2024 annual technology baseline. Available from https://atb.nrel.gov/electricity/2024b/index

Nikkho SK, Heidarinejad M, Liu JY, et al., 2017. Quantifying the impact of urban wind sheltering on the building energy consumption. *Applied Thermal Engineering*, 116:850-865. https://doi.org/10.1016/j.applthermaleng.2017.01.044

Perera ATD, Nik VM, Mauree D, et al., 2017. Electrical hubs: An effective way to integrate non-dispatchable renewable energy sources with minimum impact to the grid. *Applied Energy*, 190:232-248. https://doi.org/10.1016/j.apenergy.2016.12.127

Perera ATD, Nik VM, Chen DL, et al., 2020. Quantifying the impacts of climate change and extreme climate events on energy systems. *Nature Energy*, 5(2):150-159. https://doi.org/10.1038/s41560-020-0558-0

Perera ATD, Javanroodi K, Nik VM, 2021. Climate resilient interconnected infrastructure: Co-optimization of energy systems and urban morphology. *Applied Energy*, 285:17. https://doi.org/10.1016/j.apenergy.2020.116430

Perera ATD, Javanroodi K, Mauree D, et al., 2023. Challenges resulting from urban density and climate change for the eu energy transition. *Nature Energy*, 8(4):397-412. https://doi.org/10.1038/s41560-023-01232-9

Ran JY, Qiu YB, Liu JZ, et al., 2024a. Coordinated

optimization design of buildings and regional integrated energy systems based on load prediction in future climate conditions. *Applied Thermal Engineering*, 241:16. https://doi.org/10.1016/j.applthermaleng.2024.122338

Ran JY, Song Y, Zhou SY, et al., 2024b. A bi-level optimization method for regional integrated energy system considering uncertainty and load prediction under climate change. *Journal of Building Engineering*, 84:20. https://doi.org/10.1016/j.jobe.2024.108527

Rodrigues E, Fernandes MS, Carvalho D, 2023. Future weather generator for building performance research: An open-source morphing tool and an application. *Building and Environment*, 233:13. https://doi.org/10.1016/j.buildenv.2023.110104

Salvati A, Monti P, Roura HC, et al., 2019. Climatic performance of urban textures: Analysis tools for a mediterranean urban context. *Energy and Buildings*, 185:162-179. https://doi.org/10.1016/j.enbuild.2018.12.024

Salvati A, Kolokotroni M, 2023. Urban microclimate and climate change impact on the thermal performance and ventilation of multi-family residential buildings. *Energy and Buildings*, 294:16. https://doi.org/10.1016/j.enbuild.2023.113224

Santamouris M, Georgakis C, Niachou A, 2008. On the estimation of wind speed in urban canyons for ventilation purposes - part 2: Using of data driven techniques to calculate the more probable wind speed in urban canyons for low ambient wind speeds. *Building and Environment*, 43(8):1411-1418. https://doi.org/10.1016/j.buildenv.2007.01.042

Shen PY, Liu JH, Wang ML, 2021. Fast generation of microclimate weather data for building simulation under heat island using map capturing and clustering technique. *Sustainable Cities and Society*, 71:20. https://doi.org/10.1016/j.scs.2021.102954

Shi YR, Xiang YR, Zhang YF, 2019. Urban design factors influencing surface urban heat island in the high-density city of guangzhou based on the local climate zone. *Sensors*, 19(16):20. https://doi.org/10.3390/s19163459

State Grid Zhejiang Electric Power Company Limited. 2024. Announcement of state grid zhejiang electric power co. Ltd. On acting industrial and commercial power purchase prices for february 2024. Available from https://csc-static.sgcc.com.cn:28888/omg-static/993012819090466629041009444325541.html

Stewart ID, Oke TR, 2012. Local climate zones for urban temperature studies. *Bulletin of the American Meteorological Society*, 93(12):1879-1900. https://doi.org/https://doi.org/10.1175/BAMS-D-11-00019.1

Tamer T, Dino IG, Akgul CM, 2022. Data-driven, long-term prediction of building performance under climate change: Building energy demand and bipv energy generation analysis across turkey. *Renewable & Sustainable Energy Reviews*, 162:17. https://doi.org/10.1016/j.rser.2022.112396

Taylor KE, 2001. Summarizing multiple aspects of model performance in a single diagram. *Journal of Geophysical Research-Atmospheres*, 106(D7):7183-7192. https://doi.org/10.1029/2000jd900719

Tian C, 2021. Research and optimization of wind-solar power generation and hybrid energy storage systems. Jilin University,

Tootkaboni MP, Ballarini I, Zinzi M, et al., 2021. A comparative analysis of different future weather data for building energy performance simulation. *Climate*, 9(2):16. https://doi.org/10.3390/cli9020037

Tsoka S, Velikou K, Tolika K, et al., 2021. Evaluating the combined effect of climate change and urban microclimate on buildings' heating and cooling energy demand in a mediterranean city. *Energies*, 14(18):23. https://doi.org/10.3390/en14185799

U.S. Department of Energy. 2021. Energyplus version 9.6.0 documentation engineering reference. Available from https://energyplus.net/documentation

Wang X, 2023. Study on operation optimization of integrated energy system considering source-load uncertainty under climate change. North China Electric Power University,

Xuan WD, Ma C, Kang LL, et al., 2017. Evaluating historical simulations of cmip5 gcms for key climatic variables in zhejiang province, china. *Theoretical and Applied Climatology*, 128(1-2):207-222. https://doi.org/10.1007/s00704-015-1704-7

Yang JJ, Zhang QL, Peng CY, et al., 2024. Autobps-prototype: A web-based toolkit to automatically generate prototype building energy models with customizable efficiency values in china. *Energy and Buildings*, 305:15. https://doi.org/10.1016/j.enbuild.2023.113880

Yang XS, Peng LLH, Jiang ZD, et al., 2020. Impact of urban heat island on energy demand in buildings: Local climate zones in nanjing. *Applied Energy*, 260:13. https://doi.org/10.1016/j.apenergy.2019.114279

Yin S, Xiao SY, Ding XT, et al., 2024. Improvement of spatial-temporal urban heat island study based on local climate zone framework: A case study of hangzhou, china. *Building and Environment*, 248:18. https://doi.org/10.1016/j.buildenv.2023.111102

Yoshino H, Hong TZ, Nord N, 2017. Iea ebc annex 53: Total energy use in buildings analysis and evaluation methods. *Energy and Buildings*, 152:124-136. https://doi.org/10.1016/j.enbuild.2017.07.038

Zhang Z, 2023. Design optimization and comprehensive evaluation of hybrid renewable energy systems in urban communities. Zhejiang University,

Zhang ZL, 2024. Optimization configuration ofcarbon neutral energy system considering climate change, hybrid residual energy utilization, and market incentives. Nanchang University,

Zhao X, Ma XW, Chen BY, et al., 2022. Challenges toward carbon neutrality in china: Strategies and countermeasures. *Resources Conservation and Recycling*,

176:9. https://doi.org/10.1016/j.resconrec.2021.105959
Zou JW, Lu HY, Shu C, et al., 2023. Multiscale numerical assessment of urban overheating under climate projections: A review. *Urban Climate*, 49:24. https://doi.org/10.1016/j.uclim.2023.101551
Zou YK, Xiang K, Zhan QS, et al., 2021. A simulation-based method to predict the life cycle energy performance of residential buildings in different climate zones of china. *Building and Environment*, 193:12. https://doi.org/10.1016/j.buildenv.2021.107663

Electronic supplementary materials

Table S1-S5, Fig. S1-S4, Section S1-S5